Energy

Biomass-to-energy integrated trigeneration system using supercritical CO2 and modified Kalina cycles: energy and exergy analysis

--Manuscript Draft--

Manuscript Number:	
Article Type:	Full length article
Keywords:	S-CO2 power cycle; Kalina cycle; biomass gasification; parametric study; thermodynamic modeling
Corresponding Author:	Anna Skorek-Osikowska, Professor Silesian University of Technology Gliwice, POLAND
First Author:	Ali Shokri Kalan
Order of Authors:	Ali Shokri Kalan
	Shadab Heidarabadi
	Mohammad Khaleghi
	Hamed Ghiasirad
	Anna Skorek-Osikowska, Professor
Abstract:	One of the main global challenges is to produce energy in a sustainable way, for example, from renewable energy sources. This study proposes a novel system for trigeneration of cold, heat, and electricity, driven by biomass gasifier. The proposed solution consists of a modified Kalina cycle and a supercritical CO 2 power cycle. The input energy of the system is provided by the gasification of municipal solid waste. In addition to electricity generation, the cold is produced at the sub-zero temperature in the modified Kalina cycle, and the absorbed heat is recovered by a heating unit in the supercritical CO 2 cycle. The high thermal energy of the exhaust gases is used to increase the temperature of CO 2 entering a gas turbine and then is directed to a boiler to run the Kalina cycle. The thermodynamic relations governing the gasifier, CO 2 and Kalina cycles are developed using the engineering equation solver (EES) software. As a result of thermodynamic modeling, from 3.683 kg/s of biomass the energy and exergy efficiency at 71.75% and 55.43% can be achieved, respectively. Furthermore, the highest exergy loss is found to be 7.604 and 2.839 kW in the gasifier and combustion chamber, respectively.
Suggested Reviewers:	Dawid Hanak, PHD Senior Lecturer in Energy and Process Engineering, Cranfield University d.p.hanak@cranfield.ac.uk He is an expert in energy systems simulations and thermodynamic evaluation of power generation technologies.
	Paweł Gładysz, PhD AGH University of Science and Technology pawel.gladysz@agh.edu.pl Is an expert in process modeling and simulation of power generation systems
	Davide Bonalumi, PhD Polytechnic of Milan davide.bonalumi@polimi.it He is an expert in process simulation of power systems.

Biomass-to-energy integrated trigeneration system using supercritical CO_2 and modified Kalina cycles: energy and exergy analysis

Ali Shokri Kalan[a], Shadab Heidarabadi[a], Mohammad Khaleghi[a], Hamed Ghiasirad[b], Anna Skorek-Osikowska[b,*]

[a]*Faculty of Mechanical Engineering, Sahand University of Technology, Sahand New Town, Tabriz, Iran*

[b]*Silesian University of Technology, Faculty of Energy and Environmental Engineering, Department of Power Engineering and Turbomachinery, ul. Konarskiego 18, 44-100 Gliwice, Poland*

** Corresponding author's email address and telephone number: anna.skorek@polsl.pl +48322372524 (Anna Skorek-Osikowska)*

Co-authors email addresses: a_shokri@sut.ac.ir (Ali Shokri Kalan), shadab.heidarabadi@gmail.com (Shadab Heidarabadi), m.khaleghi737@gmail.com (Mohammad Khaleghi), hamed.ghiasirad@polsl.pl (Hamed Ghiasirad)

Keywords: S-CO_2 power cycle, Kalina cycle, biomass gasification, parametric study, thermodynamic modeling

Abstract

One of the main global challenges is to produce energy in a sustainable way, for example, from renewable energy sources. This study proposes a novel system for trigeneration of cold, heat, and electricity, driven by biomass gasifier. The proposed solution consists of a modified Kalina cycle and a supercritical CO_2 power cycle. The input energy of the system is provided by the gasification of municipal solid waste. In addition to electricity generation, the cold is produced at the sub-zero temperature in the modified Kalina cycle, and the absorbed heat is recovered by a heating unit in the supercritical CO_2 cycle. The high thermal energy of the exhaust gases is used to increase the temperature of CO_2 entering a gas turbine and then is directed to a boiler to run the Kalina cycle. The thermodynamic relations governing the gasifier, CO_2 and Kalina cycles are developed using the engineering equation solver (EES) software. As a result of thermodynamic modeling, from 3.683 kg/s of biomass the energy and exergy efficiency at 71.75% and 55.43% can be achieved, respectively. Furthermore, the highest exergy loss is found to be 7.604 and 2.839 kW in the gasifier and combustion chamber, respectively.

Nomenclature

AF	Air-fuel ratio
c_P	Specific heat at constant pressure (kJ/kgK)
$\dot{E}$	Exergy rate (kW)
f	Circulation ratio
h	Specific enthalpy (kJ/kg)
$\bar{h}$	Molar specific enthalpy (kJ/kmol)
LHV	Lower heating value (kJ/kg
$L\bar{H}V$	Molar lower heating value (kJ/kmol)
M	Molecular weight (kg/kmol)
MC	Moisture content (%)
$\dot{m}$	Mass flow rate (kg/s)
$\dot{n}$	Mole flow rate (kmol/s)
P	Pressure (bar)
$\dot{Q}$	Heat transfer rate (kW)
qu	Quality (kg/kg)
$\bar{R}$	General gas constant (kJ/kmolK)
s	Specific entropy (kJ/kgK)
SR	Split ratio
T	Temperature (K)
u	Internal energy (kJ)
$\dot{W}$	Electrical power (kW)
X	Ammonia mass fraction (%)
y_d	Exergy destruction ratio (%)

Greek symbols

$\mathbf{\Delta}$	Difference
η_{I}	Energy efficiency (%)
η_{II}	Exergy efficiency (%)
β	Chemical exergy coefficient of biomass
φ	Equivalence ratio

Subscripts and superscripts

Amb	Ambient
cr	Critical
ch	Chemical
cw	Cooling water
D	Destruction
exh	Exhaust gases
F	Fuel exergy
f	Formation
i	Inlet
isen	Isentropic
j	Outlet
k	k^{th} component
L	Exergy loss
ph	Physical
P	Product exergy
PP	Pinch Point
sat	Saturated state
S-CO_2	Supercritical carbon dioxide
th	Thermo-mechanical
0	Dead state

1. Introduction

Using fossil fuels causes significant air pollution, which is a major contributor to global warming. When fossil fuels are burned, air pollutants are released, which can be detrimental to public health and the environment. The emissions of sulfur dioxide resulting from coal burning accelerate acid rains, an important contributor to harmful particulate matter formation. Moreover, fossil fuel reserves are finite, and they will eventually be depleted. To reduce human dependence

on them, many studies have been conducted in order to replace fossil fuels with renewable energy sources (RES) such as solar energy, wind energy, geothermal energy, wave energy and biomass [1]. Biomass fuels, such as wood, waste straw, municipal solid waste (MSW), sawdust, and paddy husk, can be easily gasified, giving potential to produce energy (electricity and heat) or biofuels in a sustainable way [2,3].

In addition to replacing the nonrenewable fuels with renewable alternatives such as biomass, high efficiency energy conversion systems are essential for addressing the energy crisis and global warming issues. In this regard many efficient cycles such as Rankine cycle [4], Stirling cycle [5], supercritical CO_2 (s-CO_2) cycle [6], Kalina cycle [7] and now combination of them [8] have been developed and used. Moreover, many studies focused on trigeneration systems instead of conventional energy systems owing to their higher efficiency. Therefore, a trigeneration system fueled with biomass could be an alternative for the fossil fuel conversion solutions [9].

Huang et al. [10] examined a small-scale biomass-fed trigeneration system including a biomass combustion unit, an organic Rankine cycle (ORC), and an absorption cooling device. Compared to a simple ORC, trigeneration systems are able to enhance energy efficiency from 11% to 71% and reduce the price of electricity by 53%. He et al. [11] proposed a biomass-driven heat conversion system consisting of biomass gasification, a Stirling engine, a gas turbine, and a supercritical CO_2 cycle combined with a local water heater. The developed system was analyzed from energy, exergy and exergoeconomic perspectives. It was found that utilization of municipal solid waste as an input led to the highest energy efficiency and the lowest CO_2 emissions. Furthermore, the system with the Stirling engine has lower CO_2 emission and higher energy efficiency than the system without it. Cao et al. [12] developed a multi-generation system fueled with biomass by effectively recovering the waste heat of a combined regenerative gas turbine cycle and recompression supercritical CO_2 Brayton cycle through subsystems, such as a thermoelectric generator, a LiBre-H_2O absorption refrigeration system, a heat recovery steam generator, and a proton exchange membrane electrolyzer with the cycle. The results indicate that the use of the solar power tower results in slight reductions in environmental impacts, while significant diminutions in thermodynamic and economic performances. For hybrid and biomass-only modes, the total energy efficiency of the system improves by 22.48 and 29.6% points, respectively, and the total exergy efficiency of the system enhances by 6.18 and 7.6% points, respectively. Musharavati [13] proposed a multi-generation system including a Polymer Electrolyte Membrane (PEM) electrolyzer, a reverse osmosis desalination unit, a Kalina cycle, and a thermoelectric module that can generate power, fresh water, hot water, and hydrogen. They performed the exergy analysis and found out different locations of the system with high irreversibility. Furthermore, they indicated a parameter most affecting the performance of the system and then found out the optimal values through an optimization scheme. Ji-chao and Sobhani [14] developed an innovative polygeneration system integrated with biomass fuels by combining a gas turbine cycle, a supercritical CO_2 cycle, and a Kalina cycle. Then, they examined the performance of the system through energy and exergy analysis. According to the findings, the energy and exergy efficiencies of the system are equal to 78.15% and 40.97%, respectively. In addition, heating capacity enhanced with the increment of air preheater's terminal temperature difference (ΔTAP), air compressor's pressure ratio (r_{1p}), and pressure ratio of supercritical CO_2

cycle (s-CO_2) compressor (r_{2p}). Besides, the minimum value of SUCP was obtained for the air compressor pressure ratio of r_{1p}=13.24 and r_{2p}=2.63. The maximum value of exergy efficiency was calculated at ΔTAP=262 K, r_{1p}=14.5, and r_{2p}=4.21. Moreover, the maximum net output power was obtained when the design parameters were set as ΔTAP=262 K, r_{1p}=14.5, and r_{2p}=3.5. Shokri Kalan et al. [15] developed an innovative combined cooling and power system consisting of modified Kalina cycle and double-effect absorption refrigeration cycle by recovering the waste heat of an internal combustion engine. According to their results, boiler and turbine were the most destructive equipment, and the exergy efficiency of absorber 2, preheater 2 and sub-cooler found to be less than 40%. Fan and Dai [16] combined recompression s-CO_2 cycle and simple s-CO_2 cycle with Kalina power cycle to achieve higher efficiency in energy conversion for nuclear power plants. The results show that the RSC-Kalina cycle always performs better than the SSC-Kalina cycle and can improve the exergy efficiency (η_{ex}) by 6.37% and 7.53%, compared to the independent cycles - RSC and SSC, respectively. Compared to the valve control strategy, the compressor control strategy enables the variable speed RSC-Kalina cycle to achieve higher efficiencies under partial factory loads, from 29.67% to 58.24% under relative factory loads of 10-100%. Using the slip pressure control strategy, regardless of which s-CO_2 control strategy is adopted, the Kalina cycle can be well adapted to changes in the coating cycle parameters. Gholamian et al. [17] proposed a poly-generation system including a domestic water heater, a gas turbine, biomass gasifier and a s-CO_2 cycle. They demonstrated that gasifier and combustion chamber (CC) significantly contributed to exergy destruction. Wang et al. [18] investigated the thermodynamics of a biomass-fueled combined cooling, heating, and power system. The system consisted of a gasifier, an internal combustion engine and absorption refrigeration unit. In addition, two heat exchangers were used to heat the water and recover the waste heat from the flue gas. The system was analyzed at three different operating periods: summer, winter, and transitional seasons. According to the results, the system efficiency is 50% in the summer, 37% in winter, and 36% in the transitional season. Moreover, the gasifier accounted for 70% of the total energy and exergy losses, contributing the most to energy and exergy destruction.

Gasification of biomass is one of the most widely used thermochemical conversion methods for producing renewable energy, fuels, and biochar. This study presents a novel trigeneration system for heat, cold and electricity production. The proposed system involves biomass gasification, a supercritical CO_2 cycle and a Kalina cycle. Utilizing a modified Kalina cycle together with s-CO_2 cycle is a key advantage of the proposed system. To increase the system's flexibility under different operating conditions, the Kalina cycle uses an ammonia-water mixture as the working fluid. Since the ammonia-water mixture vaporizes non-isothermally, the Kalina cycle is better than the conventional Rankine cycle. Despite this, the feasibility of the devised biomass-powered cooling and power system has not been investigated. Proposing a novel combined cooling, heating and power generation (CCHP) system including a biomass gasifier, Kalina cycle, s-CO_2 cycle, and utilization of supercritical carbon dioxide for further power generation, energy, exergy evaluation of the proposed system are the most notable contributions of this work.

The main novelties of the proposed system can be summarized as follows:

- Using a reboiler heater and a heating unit in s-CO_2 power cycle rather than a condenser,

- Serial configuration of syngas stream to recover more thermal energy,
- Carbon dioxide utilization in the first cycle,
- Energy and exergy analysis to improve the most destructive subsystems,
- Combining two efficient cycles to meet cooling, heating, and power demands,
- Using municipal solid waste gasification as an alternative energy sources,
- Conducting parametric study using net output power and exergy efficiency as objective functions in order to find the decision variables.

2. Methods

2.1. Description of the proposed system

A schematic diagram of the proposed system is given in 0. As can be seen from this figure, the system consists of three subsystems including gasifier, supercritical CO_2 (s-CO_2) cycle and Kalina cycle. In the gasification process, the air (state 58, Fig. 1), which plays the role of the gasification agent, and biomass (59), are fed to the gasifier where the gasification process occurs and the syngas (39) is produced. Then, together with the air (38), they are fed to the combustion chamber (CC). To supply the primary energy for the Kalina cycle, the high-temperature combustion chamber's exhaust gases (40) are directed to the boiler (41) after passing through the generator (GEN) which is used to increase the turbine inlet temperature (TIT) in the s-CO_2 cycle (44).

In the s-CO_2 cycle, heated CO_2 (state 44) passes through the turbine 1 to generate electrical power. Afterwards, to preheat CO_2 return flow, it (45) is passed through the high-temperature recuperator and subsequently low-temperature recuperator (denoted, respectively, by HTR and LTR in Fig. 1) before being split into two parts. One part of the stream (49) is pre-heated in LTR after passing through the reboiler section of distillation column and then compressed in main compressor (MC), and the other (48) goes toward recompressor (RC). The two streams (52 and 53) are mixed before being heated in the HTR.

The Kalina cycle includes three main subsystems of high-pressure, low-pressure and medium pressure. In the high-pressure subsystem, the ammonia-water mixture at the outlet of the absorber 2 (8) is split into two parts: one part (8″) is pumped by the pump 3 and subsequently pre-heated in the preheater 2, and finally directed to the rectifier section of distillation column. The other part of the stream (8′) is directed to the boiler after passing from high-pressure pump (pump 2) and subsequently pre-heated in preheater 1 (powered by dilute solution). In the boiler the temperature of the mixture is increased and then it enters the Kalina cycle's turbine (turbine 2) where the output power is produced. In the low-pressure subsystem of the Kalina cycle, ammonia-water mixture leaving the turbine (14) is directed to the recuperator 1 where it is cooled. Then the output is mixed with dilute solution streams (6 & 27) and high concentration ammonia (24), and subsequently is passed through the low-pressure absorber (A1) to release the heat to the cooling water flow. In the medium pressure subsystem of Kalina cycle, the ammonia-water mixture (1) passes through the pump 1 before being split into two parts of lower and higher mass flow rates (state 2″ and 2′). The part with higher mass flow rate (state 2′) is preheated subsequently in recuperators 1 and 2, and then is directed to the separator where the mixture is split into two parts of a weak mixture (4′) and

a rich mixture (4″). The weak mixture is used to preheating the ammonia-water mixture before entering boiler and then it is directed to the mixer after passing the valve 2. The rich mixture flows through preheater 2, where it is cooled, mixed with low concentration ammonia stream (2″) and then is directed to the absorber 2.

The distillation column comprises three sections of reboiler, rectifier, and partial condenser. The main task of the rectifier, which is the middle part of the distillation column and includes several trays (mainly porous trays), is mixture separation and rectification. The input mixture (18) to this section is separated into two parts of liquid and vapor. They are directed to the lower and upper sections of distillation column, respectively. The liquid part which enters the reboiler is heated and the generated vapor is directed to the condenser section. The output of the condenser part of distillation column (19) enters the evaporator (22) for further cooling after releasing heat in the subcooler (21); subsequently, it turns back to the subcooler and then flows to the mixer (24). The diluted mixture that exits the reboiler (25) heats the basic mixture in the recuperator 2 and then flows toward the mixer through the valve 4.

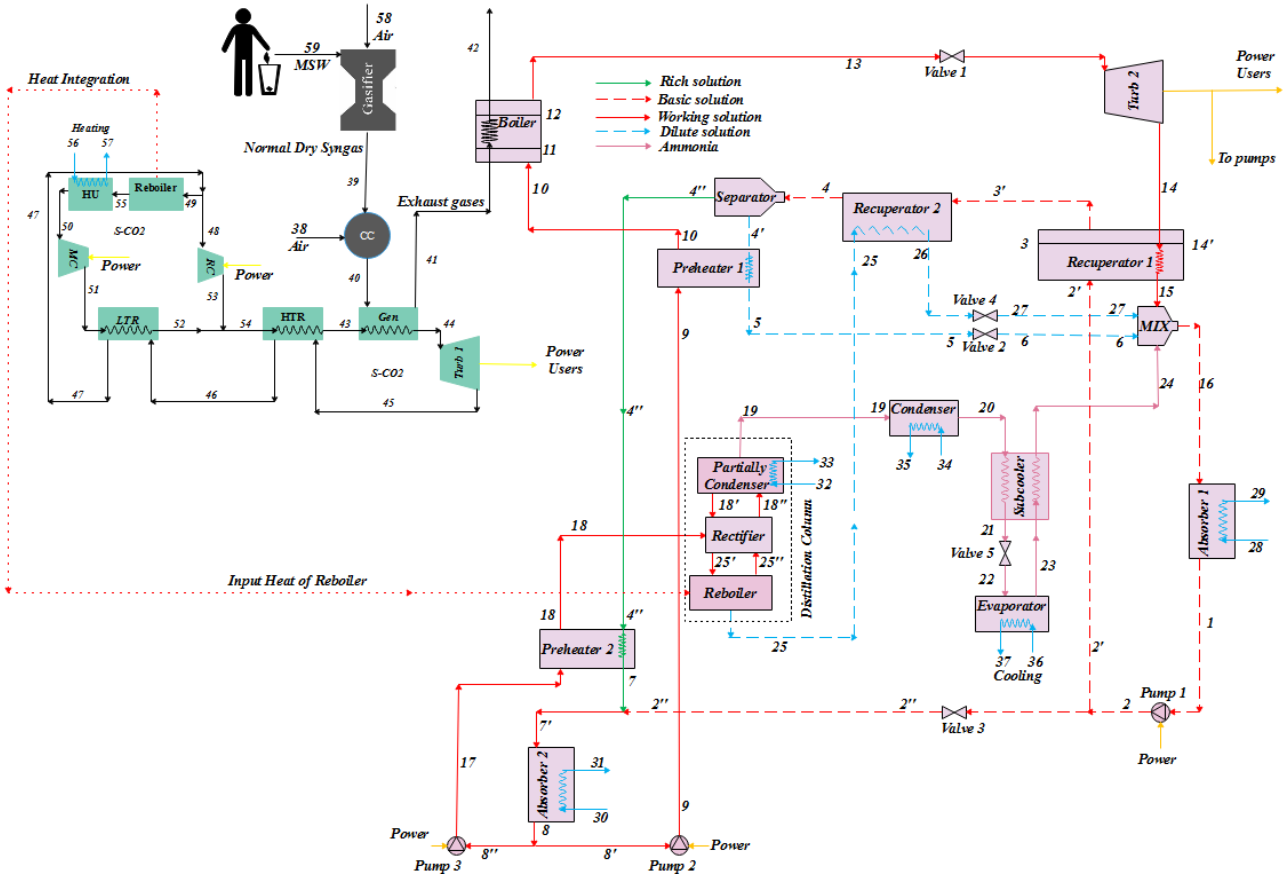

Figure 1. Schematic diagram of the proposed biomass-based trigeneration system

In order to model the proposed system from energy and exergy viewpoints, the necessary input data are reported in Table 1.

Table 1. Input data for thermodynamic modelling of the proposed system

Input data	Unit	Value	Ref.
Ambient temperature	K	298.15	[19]
Ambient pressure	bar	1.013	[19]
Gasifier and combustion reactions			
LHV of biomass	kJ/kg	13980	[20]
The heat of formation	kJ/kmol	-221579	[20]
Mass flow rate of biomass	Kg/s	1.155	[20]
Syngas temperature	K	823.15	[20]
Syngas mass flow rate	kg/s	3.683	[20]
Moisture content	(wt.%)	14.93	[20]
Chemical composition of MSW	-	$CH_{1.46}O_{0.69}$	[20]
Molar equivalence ratio	-	0.7	[21]
O_2 mole fraction in air	%	21	[21]
N_2 mole fraction in air	%	79	[21]
S-CO_2 power cycle			
Pressure ratio of compressors	bar	5	[19]
Maximum temperature of s-CO_2	K	818.15	[22]
Isentropic efficiency of turbine and compressors	%	84	[23]
Effectiveness of heat exchangers	%	84	[23]
Pressure drop in generator and LTR	%	2	[24]
Pressure drop in HTR	%	3	[24]
Pressure drop in reboiler and HU	%	1	[24]
Pinch point temperature difference of generator	K	3	[25]
Output pressure of s-CO_2 turbine	bar	75	[19]
Split ratio of s-CO_2	-	0.3	[19]
Inlet temperature of MC	K	300.65	[26]
Kalina cycle			
Pinch point temperature difference of heat exchangers	K	3	[25]
Input temperature of boiler, T_{10}	K	344.65	[15]
Output pressure of pump 2	bar	86.26	[15]
Ammonia concentration in absorber 2	-	0.5	[15]
Inlet temperature of Kalina turbine	K	653.15	[15]
Isentropic efficiency of pumps	%	85	[27]
Isentropic efficiency of Kalina turbine	%	90	[28]
Split fraction ratio, f_w	-	0.57	[28]
Temperature at the bottom of distillation column, T_{25}	K	398.15	[28]
Pressure at the bottom of distillation column, P_{25}	bar	13.48	[28]
Vapor fraction at the bottom of distillation column, Qu_{25}	-	0	[28]
Rectifier efficiency	%	70	[28]
Outlet temperature of cooling water streams	K	303.15	[4]
Inlet water temperature of evaporator	K	260	[28]
Outlet water temperature of evaporator	K	255.15	[28]

Terminal temperature difference of HU	K	30	[29]

2.2. Mathematical model of the proposed system

In this section, the thermodynamic models of the main subsystems of the proposed cycle, including gasifier, combustion chamber, s-CO_2 cycle and Kalina Cycle are described. The following assumptions are considered:

- The transient response is not considered; therefore, all components of the system works in steady-state conditions.
- There is no leakage of working fluid in the system.
- The kinetic and potential energies are negligible.
- Pressure drops in heat exchangers and pipelines as well as heat transfer between the system and the environment are neglected.

The main tools for mathematical modeling of the proposed system are conservation of energy and mass. Generally, by applying the energy and mass balance for a component, the following equations can be written [30]:

$$\dot{Q} - \dot{W} + \sum_{\mathrm{i}} \dot{m}_{\mathrm{i}} \left(h_{\mathrm{i}} + \frac{V_{\mathrm{i}}^2}{2} + g z_{\mathrm{i}} \right) - \sum_{\mathrm{e}} \dot{m}_{\mathrm{e}} \left(h_{\mathrm{e}} + \frac{V_{\mathrm{e}}^2}{2} + g z_{\mathrm{e}} \right) = \frac{dE}{dt} \tag{1}$$

$$\sum_{\mathrm{i}} \dot{m}_{\mathrm{i}} = \sum_{\mathrm{i}} \dot{m}_{\mathrm{e}} \tag{2}$$

Also, by neglecting changes in the potential and kinetic energies, the physical exergy is obtained from the following relation [31]:

$$e_{\mathrm{ph}} = h - h_0 - (T_0)(s - s_0) \tag{3}$$

The specific molar chemical exergy of a mixture of ideal gases is defined as below [31]:

$$\bar{e}^{\mathrm{Ch}}_{\mathrm{Mixture}} = \sum_{i} X_{\mathrm{i}}\, \bar{e}^{\mathrm{Ch}}_{\mathrm{i}} + \bar{R} T_0 \sum_{i} X_{\mathrm{i}} ln X_{\mathrm{i}} \tag{4}$$

In which, X_{i} and $\bar{e}^{\mathrm{Ch}}_{\mathrm{i}}$ define the mole fraction and the standard chemical exergy of a mixture component, respectively. The standard chemical exergy of some substances is given in Ref. [31]

$$\dot{E} = \dot{m}(e_{\mathrm{ph}} + e_{\mathrm{ch}}) \tag{5}$$

All the components of the system are explicitly modelled using the above balance equations. Details of this modelling are given below.

2.2.1. Gasifier subsystem

Error! Reference source not found. provides the chemical formula of biomass (municipal solid wastes) used for calculating lower heating value of biomass. To represent the chemical reactions for the gasification process, the following global equation is used [32]:

$$\left(\mathrm{CH_xO_y} + \mathrm{wH_2O}\right) + m(0.21\mathrm{O_2} + 0.79\mathrm{N_2}) \rightarrow a_1\mathrm{H_2} + a_2\mathrm{CO} + a_3\mathrm{CO_2} + a_4\mathrm{H_2O} + a_5\mathrm{CH_4} + a_6\mathrm{N_2} \quad (6)$$

where, m represents the air to biomass molar ratio and a_1, a_2, a_3, a_4, a_5 and a_6 are the mole numbers of the syngas species formed per mole of the consumed feedstock. Furthermore, the mole number of the feedstock moisture, w, can be calculated from the following equation [32]:

$$w = \frac{MW_{\mathrm{Biomass}} \cdot MC}{MW_{\mathrm{H2O}} \cdot (1 - MC)} \quad (7)$$

where MW and MC refer to the molecular weight and moisture content, respectively.

To find out the 7 unknown parameters, i.e., m, a_1, a_2, a_3, a_4, a_5 and a_6 in equation (6), 7 equations are needed. The energy conservation equation and the equilibrium constants of methane formation reaction and water gas shift reaction are used along with mass balance equations for carbon, hydrogen, oxygen, and nitrogen. From the mass balances of carbon, hydrogen, oxygen, and nitrogen, the following equations can be derived:

$$a_2 + a_3 + a_5 = 1 \quad (8)$$

$$2a_1 + 2a_4 + 4a_5 = 1.46 + 2w \quad (9)$$

$$a_2 + 2a_3 + a_4 = 0.69 + w + 0.42m \quad (10)$$

$$a_6 = 0.79\, m \quad (11)$$

Establishing the energy balance for the gasification process provides another equation can be written as follows:

$$a_1\bar{h}^0_{\mathrm{H_2}} + a_2\bar{h}^0_{\mathrm{CO}} + a_3\bar{h}^0_{\mathrm{CO_2}} + a_4\bar{h}^0_{\mathrm{H_2O}} + a_5\bar{h}^0_{\mathrm{CH_4}} + a_6\bar{h}^0_{\mathrm{N_2}} - \bar{h}^0_{\mathrm{f,biomass}} - w\bar{h}^0_{f,\mathrm{H_2O(l)}} - m\left(0.21\bar{h}^0_{\mathrm{f,O_2}} + 0.79\bar{h}^0_{\mathrm{f,N_2}}\right) = \dot{Q}_{\mathrm{l,Gasifier}} \quad (12)$$

where, $\bar{h}^0_{\mathrm{f,biomass}}$, $\bar{h}^0_{\mathrm{f,H_2O(l)}}$, $\bar{h}^0_{\mathrm{f,O_2}}$ and $\bar{h}^0_{\mathrm{f,N_2}}$ are the formation heat of biomass feedstock, liquid water, oxygen, and nitrogen, respectively. Additionally, $\bar{h}^0$ indicates the molar absolute enthalpy of each species of the produced gas in the standard pressure and the gasifier temperature [20] and $Q_{\mathrm{l,Gasifier}}$ denotes heat losses from gasifier.

In the reduction zone of the gasifier, several reactions including solid-carbon reaction, Boudouard reaction, water – gas shift reaction, and methane formation reaction occurs. They can, respectively, be written as [33]:

$$\begin{gathered} \mathrm{C} + \mathrm{H_2O} \leftrightarrow \mathrm{CO} + \mathrm{H_2} \\ C + \mathrm{CO_2} \leftrightarrow 2\,\mathrm{CO} \\ \mathrm{CO} + \mathrm{H_2O} \leftrightarrow \mathrm{CO_2} + \mathrm{H_2} \\ \mathrm{C} + 2\,\mathrm{H_2} \leftrightarrow \mathrm{CH_4} \end{gathered} \tag{13}$$

In this paper, the water-gas shift and methane reactions are the ones considered among all reactions taking place in the reduction zone. Equilibrium constants for water-gas shift and methane reactions can be obtained using the following stoichiometric coefficients, respectively [33]:

$$K_1 = \frac{P_{\mathrm{CO2}} \cdot P_{\mathrm{H2}}}{P_{\mathrm{CO}} \cdot P_{\mathrm{H2O}}} = \frac{a_3 \cdot a_1}{a_2 \cdot a_4} \tag{14}$$

$$K_2 = \frac{P_{\mathrm{CH4}}}{{P_{\mathrm{H2}}}^2} = \frac{a_5 \cdot (a_1 + a_2 + a_3 + a_4 + a_5 + a_6)}{{a_1}^2} \tag{15}$$

where, P_i denotes the partial pressure for each gas constituent (i). The equilibrium constants can be expressed in terms of Gibbs free energy of chemical reaction, as shown below:

$$K_{\mathrm{i}}(T_{\mathrm{Gasifier}}) = exp\left[-\frac{\Delta \bar{g}_i}{\bar{R} T_{\mathrm{Gasifier}}}\right] (i = 1{,}2) \tag{16}$$

in which $\bar{R}$ is the universal gas constant, equal to 8.314 kJ/kmol/K, and T_{Gasifier} is gasification temperature. Furthermore, $\Delta \bar{g}_i$ are calculated for the equilibrium reactions as below [34]:

$$\Delta \bar{g}_{\mathrm{i}} = \Delta \bar{h}_{\mathrm{i}} - T_{\mathrm{Gasifier}} \Delta \bar{s}_{\mathrm{i}} \tag{17}$$

where:

$$\Delta \bar{h}_1 = \bar{h}^0_{\mathrm{CO_2}} + \bar{h}^0_{\mathrm{H_2}} - \bar{h}^0_{\mathrm{CO}} - \bar{h}^0_{\mathrm{H_2O}} \tag{18}$$

$$\Delta \bar{h}_2 = \bar{h}^0_{\mathrm{CH_4}} - 2\bar{h}^0_{\mathrm{H_2}} - \bar{h}^0_{\mathrm{C}} \tag{19}$$

$$\Delta \bar{s}_1 = \bar{s}^0_{\mathrm{CO_2}} + \bar{s}^0_{\mathrm{H_2}} - \bar{s}^0_{\mathrm{CO}} - \bar{s}^0_{\mathrm{H_2O}} \tag{20}$$

$$\Delta \bar{s}_2 = \bar{s}^0_{\mathrm{CH_4}} - 2\bar{s}^0_{\mathrm{H_2}} - \bar{s}^0_{\mathrm{C}} \tag{21}$$

To enhance the accuracy of the modeling results, the coefficients A_1 and A_2 are multiplied by the equilibrium constants. These coefficients are derived from the ratios of the constituent fractions of the present model to those of experimental models [35].

In order to assess the effectiveness of the gasification process cold gas efficiency (η_{CG}) is used. Cold gas efficiency is defined as the ratio of the chemical energy of the produced syngas to the

total input energy, which is equivalent to the chemical energy of the biomass fed to the gasifier [36]:

$$\eta_{\mathrm{CG}} = \frac{\dot{m}_{\mathrm{Pro.Gas}} LHV_{\mathrm{Pro.Gas}}}{\dot{m}_{\mathrm{Biomass}} LHV_{\mathrm{Biomass}}} \tag{22}$$

where, $\dot{m}_{\mathrm{Pro.Gas}}$ and $LHV_{\mathrm{Pro.Gas}}$ are the mass flow rate and lower heating value of the produced gas, respectively, while $\dot{m}_{\mathrm{Biomass}}$ and $LHV_{Biomass}$ are the mass flow rate and the lower heating value of biomass feedstock, respectively. Additionally, the dry gas yield (DGY) is defined as the volume of the produced gas (on dry basis) obtained per mass unit of the biomass [36]:

$$DGY = \frac{\dot{V}_{\mathrm{Dry.gas}}}{\dot{m}_{\mathrm{Biomass}}} \tag{23}$$

where $\dot{V}$and $\dot{m}$ are volume and mass flow rates, respectively.

In the literature an actual air-fuel ratio (AF_{act}) is sometimes used to assess the results of the gasification process modeling. It is calculated using the following equation:

$$AF_{\mathrm{act}} = \frac{m \cdot MW_{\mathrm{Air}}}{MW_{\mathrm{Biomass}}} \tag{24}$$

where, MW_{Air} is the molecular weight of the gasification air and *m* is the air to biomass molar ratio.

Error! Reference source not found. presents the relations concerning mass, energy and exergy balance equations for the gasifier subsystem.

Table 2. Equilibrium equations for the gasification subsystem

Mass and energy balance equations	**Exergy balance equations**		
	Fuel	Product	Loss
Presented in section 2.2.1.	$\dot{\mathrm{E}}\mathrm{x}_{58} + \dot{\mathrm{E}}\mathrm{x}_{59}$	$\dot{\mathrm{E}}\mathrm{x}_{39}$	$\dot{\mathrm{Q}}_{\mathrm{loss}}(1 - \frac{\mathrm{T}_0}{\mathrm{T}_{39}})$

2.2.2. Combustion chamber subsystem

The combustion reaction is assumed to be stoichiometric when the equivalence ratio $\varphi = 1$ and there is no oxygen in combustion products, and if $0 < \varphi < 1$ the reaction would have extra oxygen in products [21]:

$$(Syngas) + \frac{A_{\mathrm{Stoich}}}{\varphi}(0.21\mathrm{O}_2 + 0.79\mathrm{N}_2) \longrightarrow \left[X_{\mathrm{CO}_2}\mathrm{CO}_2 + X_{\mathrm{H}_2\mathrm{O}}\mathrm{H}_2\mathrm{O} + X_{\mathrm{O}_2}\mathrm{O}_2 + X_{\mathrm{N}_2}\mathrm{N}_2\right] \tag{25}$$

Stoichiometric air (A_{Stoich}) should be found beforehand, then by assumingφ, eq. (22) can be solved to find X_{i} which denotes the combustion products mole fraction. In this equation, the equivalence ratio (φ) is defined as:

$$\varphi = AF_{Stoich}/AF_{Actual} \tag{26}$$

Heat losses from the combustion chamber are assumed to be 2% of the total chemical energy of the fuel mixture [21]. Therefore, it can be written that:

$$\dot{Q}_{\mathrm{Loss,CC}} = -0.02\dot{m}_{\mathrm{Fuel}} LHV_{\mathrm{Fuel}} \tag{27}$$

in which $\dot{m}_{\mathrm{Fuel}}$ and LHV_{Fuel} are the mass flow rate and the lower heating value of the fuel mixture, respectively.

The specific molar chemical exergy of biomass feedstock can be derived from the following equations [34]:

$$\bar{e}^{ch}_{\mathrm{Biomass}} = \beta L\bar{H}V_{\mathrm{Biomass}} \tag{28}$$

where, $L\bar{H}V_{Biomass}$ defines the molar heating value of biomass feedstock and β (coefficient for the chemical exergy of biomass) is calculated for solid fuels as follows:

$$\beta = \frac{1.044 + 0.016\frac{M_{\mathrm{H}}}{M_{\mathrm{C}}} - 0.34493\frac{M_{\mathrm{O}}}{M_{\mathrm{C}}}(1 + 0.0531\frac{M_{\mathrm{H}}}{M_{\mathrm{C}}})}{1 - 0.4124\frac{M_{\mathrm{O}}}{M_{\mathrm{C}}}} \tag{29}$$

In the above equation, M_{H}, M_{C} and M_{O} are the mass fractions of hydrogen, carbon, and oxygen in the biomass, respectively. 0 shows the relations regarding applying mass, energy and exergy balance equations for the combustion chamber. In this table, NDG indicates normal dry gas in the syngas stream.

Table 3. Mass, energy and exergy balance equations for combustion chamber subsystem

Mass and energy balance equations	**Exergy balance equations**		
	Fuel	Product	Loss
$\dot{m}_{40} = \dot{m}_{39} + \dot{m}_{38}$ $\dot{Q}_{\mathrm{in}} = \dot{m}_{\mathrm{NDG}}.LHV_{\mathrm{NDG}}$ $\dot{Q}_{\mathrm{loss}} = 0.02\dot{Q}_{\mathrm{in}}$	$\dot{E}x_{38} + \dot{E}x_{39}$	$\dot{E}x_{40}$	$\dot{Q}_{\mathrm{loss}}(1 - \frac{T_0}{T_{40}})$

2.2.3. Supercritical CO_2 cycle subsystem

The main components of supercritical CO_2 subsystem include compressors, turbines, recuperators, condenser and generator. In this subsection, the mass, energy, and exergy balance equations are given in Table 4.

Table 4. Mass, energy and exergy balance equations of s-CO_2 power cycle's components.

Units	Mass and energy balance equations	Fuel exergy	Product exergy
MC	$\dot{W}_{\mathrm{MC}} = (1-SR)\cdot \dot{m}_{\mathrm{sCO_2}}(h_{53}-h_{48})$	$\dot{W}_{MC}$	$\dot{E}_{51}-\dot{E}_{50}$
	$\dot{W}_{MC} = (1-SR)\cdot \dot{m}_{\mathrm{sCO_2}}(h_{53s}-h_{48})/\eta_{\mathrm{RC}}$		
RC	$\dot{W}_{\mathrm{MC}} = (1-SR)\cdot \dot{m}_{\mathrm{sCO_2}}(h_{53}-h_{48})$	$\dot{W}_{\mathrm{RC}}$	$\dot{E}_{53}-\dot{E}_{48}$
	$\dot{W}_{MC} = (1-SR)\cdot \dot{m}_{\mathrm{sCO_2}}(h_{53s}-h_{48})/\eta_{\mathrm{RC}}$		
S-CO_2 turbine	$\dot{W}_{\mathrm{T}} = \dot{m}_{\mathrm{sCO_2}}(h_{44}-h_{45})$	$\dot{E}_{44}-\dot{E}_{45}$	$\dot{W}_{\mathrm{T}}$
	$\dot{W}_{T} = \dot{m}_{\mathrm{sCO_2}}\eta_{\mathrm{T}}(h_{44}-h_{45,s})$		
HTR	$\dot{Q}_{\mathrm{HTR}} = \dot{m}_{\mathrm{sCO_2}}(h_{43}-h_{54})$	$\dot{E}_{45}-\dot{E}_{46}$	$\dot{E}_{43}-\dot{E}_{54}$
	$\dot{Q}_{HTR} = \dot{m}_{\mathrm{sCO_2}}(h_{45}-h_{46})$		
	$\varepsilon_{HTR} = \frac{T_{45}-T_{46}}{T_{45}-T_{54}}$		
LTR	$\dot{Q}_{\mathrm{LTR}} = SR\cdot \dot{m}_{\mathrm{sCO_2}}(h_{52}-h_{51})$	$\dot{E}_{46}-\dot{E}_{47}$	$\dot{E}_{52}-\dot{E}_{51}$
	$\dot{Q}_{LTR} = \dot{m}_{\mathrm{sCO_2}}(h_{46}-h_{47})$		
	$\varepsilon_{\mathrm{LTR}} = \frac{T_{46}-T_{47}}{T_{46}-T_{51}}$		
HU	$\dot{Q}_{\mathrm{HU}} = \dot{m}_{\mathrm{sCO_2}}(h_{55}-h_{50}) = \dot{m}_{56}(h_{57}-h_{56})$	$\dot{E}_{55}+\dot{E}_{56}$	$\dot{E}_{57}+\dot{E}_{50}$
GEN	$\dot{Q}_{\mathrm{GEN}} = \dot{m}_{\mathrm{sCO_2}}(h_{44}-h_{43}) = \dot{m}_{40}(h_{40}-h_{41})$	$\dot{E}_{40}-\dot{E}_{40}$	$\dot{E}_{44}-\dot{E}_{43}$
MIX3	$\dot{m}_{52}h_{52}+\dot{m}_{53}h_{53} = \dot{m}_{54}h_{54}$	$(\dot{E}x_{52}+\dot{E}x_{53}$	$\dot{E}x_{54}$

2.2.4. Kalina cycle subsystem

The governing equations for the processes in the distillation column are as below [15]:

$$\dot{m}_{18} = \dot{m}_{25} + \dot{m}_{19} \tag{30}$$

$$\dot{m}_{18}x_{18} = \dot{m}_{25}x_{25} + \dot{m}_{19}x_{19} \tag{31}$$

$$\dot{m}_{18}h_{18} + \dot{Q}_{\mathrm{reb}} = \dot{m}_{19}h_{19} + \dot{m}_{25}h_{25} + \dot{Q}_{\mathrm{PC}} \tag{32}$$

in which $\dot{Q}_{\mathrm{PC}}$ and $\dot{Q}_{\mathrm{reb}}$ describe the heat transfer rate in the partial condenser and the reboiler, respectively. To calculate the rectifier efficiency the following equations [15] are included:

$$R_{\min} = \frac{(x_{19} - x_{18\mathrm{v}})}{(x_{18\mathrm{v}} - x_{18\mathrm{l}})} \tag{33}$$

$$\eta_{\mathrm{R}} = \frac{R_{\min}}{R} \tag{34}$$

$$R = \frac{\dot{m}_{18'}}{\dot{m}_{19}} \tag{35}$$

where, $R_{\min}$ represents the lowest reflux ratio and $x_{18'}$ is the concentration of ammonia in the saturated solution flowing from the condenser to the rectifier in the actual reflux ratio (R). Additionally, $x_{18\mathrm{l}}$ and $x_{18\mathrm{v}}$ are the ammonia concentration in the solution flowing from the condenser to the rectifier and in the saturated vapor flowing from the rectifier to the condenser in the lowest reflux ratio ($R_{\min}$), respectively, while $\dot{m}_{18'}$ is the mass flow rate of the saturated solution flowing from the condenser to the rectifier. Moreover, η_{R} is the rectifier efficiency and is assumed to be 70%. The equations required to calculate $\dot{Q}_{\mathrm{PC}}$, $\dot{Q}_{\mathrm{reb}}$, and thermodynamic parameters of different states of the system are as bellow [15]:

$$\dot{m}_{25}(1 + R)x_{25} = \dot{m}_{19}x_{19} + \dot{m}_{19}Rx_{18'} \tag{36}$$

$$x_{18''} = \frac{(x_{18\mathrm{v}} - x_{18})}{(x_{18\mathrm{l}} - x_{18})}x_{18'} + \frac{(x_{18\mathrm{l}} - x_{18\mathrm{v}})}{(x_{18\mathrm{l}} - x_{18})}x_{18} \tag{37}$$

$$\frac{\dot{Q}_{\mathrm{pc}}}{\dot{m}_{19}} + Rh_{18'} + h_{19} = (1 + R)h_{18''} \tag{38}$$

$$\dot{Q}_{\mathrm{reb}} = \dot{m}_{49}(T_{49} - T_{55}) \tag{39}$$

$$\dot{m}_{25}h_{25} = \dot{m}_{25'}h_{25'} + \dot{Q}_{\mathrm{reb}} - \dot{m}_{25''}h_{25''} \tag{40}$$

$$\dot{Q}_{\mathrm{PC}} = \dot{m}_{18''}h_{18''} - \dot{m}_{18'}h_{18'} - \dot{m}_{19}h_{19} \tag{41}$$

$$\dot{Q}_{\mathrm{PC}} = \dot{m}_{32}c_{\mathrm{p,water}}(T_{33} - T_{32}) \tag{42}$$

in which $x_{25"}, h_{25"}$, and $\dot{m}_{25"}$ are the concentration, enthalpy, and mass flow rate of the solution flowing from the reboiler to the rectifier, and $x_{2\acute{5}}$, $h_{2\acute{5}}$, and $\dot{m}_{2\acute{5}}$, denote the concentration, enthalpy, and mass flow rate of the solution leaving the rectifier and entering the reboiler, respectively. $x_{18"}$ is the concentration of ammonia in output saturated vapor transferred from the rectifier to the condenser, in the actual reflux ratio (R) and $\dot{m}_{18"}$ is the mass flow rate of the saturated vapor flowing from the rectifier to the condenser in the actual reflux ratio (R).

In the system design, four different concentrations are considered for ammonia, which is connected directly by the parameters including circulation ratio f and the basic solution portion f_{b}. The required equations to calculate f and f_{b} are reported as below:

$$f = \frac{\dot{m}_1}{\dot{m}_8} = \frac{(x_w - x_4)}{(x_b - x_4)} \tag{43}$$

$$\frac{\dot{m}_6}{\dot{m}_8} = f - 1 \tag{44}$$

$$f_{\mathrm{b}} = \frac{\dot{m}_{2"}}{\dot{m}_8} = \frac{(x_{4"} - x_{\mathrm{w}})}{(x_{4"} - x_{\mathrm{b}})} \tag{45}$$

Also, the split fraction, f_{w}, and the refrigeration portion, f_{r}, are reported as bellows:

$$f_{\mathrm{w}} = \frac{\dot{m}_9}{\dot{m}_8} \tag{46}$$

$$f_{\mathrm{r}} = \frac{\dot{m}_{19}}{\dot{m}_{18}} = \frac{(x_{\mathrm{w}} - x_{25})}{(x_{19} - x_{25})} \tag{47}$$

$$\frac{\dot{m}_{19}}{\dot{m}_{18}} = (1 - f_{\mathrm{w}}) f_{\mathrm{r}} \tag{48}$$

where x_{w} and x_{b} are the concentration of the working and basic solution, respectively. It is worth mentioning that working solution means the stream entering the Kalina turbine to produce useful work.

Table 5 shows the relations concerning applying mass, energy and exergy balance equations for different components of Kalina cycle.

Table 5. Mass, energy and exergy balance equations for different components of Kalina cycle

Component	**Mass and energy balance equations**	**Exergy balance equations**		
		Fuel	***Product***	***Loss***
Boiler	$\dot{Q}_{\mathrm{Boiler}} = \dot{m}_{41}(h_{41} - h_{42}) = \dot{m}_{10}(h_{13} - h_{10})$	$\dot{E}x_{41}$	$\dot{E}x_{13} - \dot{E}x_{10}$	$\dot{E}x_{42}$
Turb 2	$\dot{W}_{\mathrm{Turb}} = \dot{m}_{13}(h_{13} - h_{14})$ $\eta_{\mathrm{Turb}} = \frac{(h_{13} - h_{14})}{(h_{13} - h_{14,is})}$	$\dot{E}x_{13} - \dot{E}x_{14}$	$\dot{W}_{Turb}$	---
Recuperator1	$\dot{Q}_{\mathrm{Recup1}} = \dot{m}_{14}(h_{14} - h_{15}) = \dot{m}_{2'}(h_{3'} - h_{2'})$	$\dot{E}x_{14} - \dot{E}x_{15}$	$\dot{E}x_{3*} + \dot{E}x_{2*}$	---
Recuperator2	$\dot{Q}_{\mathrm{Recup2}} = \dot{m}_{25}(h_{25} - h_{26}) = \dot{m}_{3'}(h_4 - h_{3'})$	$\dot{E}x_{25} - \dot{E}x_{26}$	$\dot{E}x_4 + \dot{E}x_{3*}$	---
Mixer	$\dot{m}_{24}h_{24} + \dot{m}_{27}h_{27} + \dot{m}_{15}h_{15} + \dot{m}_6h_6 = \dot{m}_{16}h_{16}$	$\dot{E}_{24} + \dot{E}_{27} + \dot{E}_{15} + \dot{E}_6$	$\dot{E}_{16}$	---
Absorber1	$\dot{Q}_{\mathrm{Absorb1}} = \dot{m}_{16}(h_{16} - h_1) = \dot{m}_{28}(h_{29} - h_{28})$	$\dot{E}x_{16} - \dot{E}x_1$	$\dot{E}x_{29} - \dot{E}x_{28}$	
Absorber2	$\dot{Q}_{\mathrm{Absorb2}} = \dot{m}_{7'}(h_{7'} - h_8) = \dot{m}_{30}(h_{31} - h_{30})$	$\dot{E}x_{7'} - \dot{E}x_8$	$\dot{E}x_{31} - \dot{E}x_{30}$	

Pump1	$h_2 - h_1 = v_1(P_2 - P_1)/\eta_{\text{is.Pump1}}$ $\dot{W}_{Pump1} = \dot{m}_1(h_2 - h_1)$	$\dot{W}_{\text{Pump1}}$	$\dot{E}x_2 - \dot{E}x_1$	---
Pump2	$h_9 - h_{8\prime} = v_{8\prime}(P_9 - P_{8\prime})/\eta_{\text{is.Pump2}}$ $\dot{W}_{Pump2} = \dot{m}_{8\prime}(h_9 - h_{8\prime})$	$\dot{W}_{Pump2}$	$\dot{E}x_9 - \dot{E}x_{8\prime}$	---
Pump3	$h_{17} - h_{8\prime\prime} = v_{8\prime\prime}(P_{17} - P_{8\prime\prime})/\eta_{\text{is.Pump3}}$ $\dot{W}_{\text{Pump3}} = \dot{m}_{8\prime\prime}(h_{17} - h_{8\prime\prime})$	$\dot{W}_{Pump3}$	$\dot{E}x_{17} - \dot{E}x_{8\prime\prime}$	---
Preheater1	$\dot{Q}_{\text{Preheater1}} = \dot{m}_{4\prime}(h_{4\prime} - h_5) = \dot{m}_9(h_{10} - h_9)$	$\dot{E}x_{4\prime} - \dot{E}x_5$	$\dot{E}x_{10} - \dot{E}x_9$	---
Preheater2	$\dot{Q}_{\text{Preheater2}} = \dot{m}_{4\prime\prime}(h_{4\prime\prime} - h_7) = \dot{m}_{17}(h_{18} - h_{17})$	$\dot{E}x_{4\prime\prime} - \dot{E}x_7$	$\dot{E}x_{18} - \dot{E}x_{17}$	---
Condenser1	$\dot{Q}_{\text{con1}} = \dot{m}_{19}(h_{19} - h_{20}) = \dot{m}_{34}(h_{35} - h_{34})$	$\dot{E}x_{19} - \dot{E}x_{20}$	$\dot{E}x_{35} - \dot{E}x_{34}$	---
Subcooler	$\dot{m}_{20}(h_{20} - h_{21}) = \dot{m}_{23}(h_{24} - h_{23})$	$\dot{E}x_{20} + \dot{E}x_{23}$	$\dot{E}x_{21} + \dot{E}x_{24}$	---
Evaporator	$\dot{Q}_{\text{evap}} = \dot{m}_{22}(h_{23} - h_{22}) = \dot{m}_{36}(h_{36} - h_{37})$	$\dot{E}x_{22} - \dot{E}x_{23}$	$\dot{E}x_{37} - \dot{E}x_{36}$	---
Throttle valve 2,4,5	$h_{26} = h_{27}$, $h_5 = h_6$, $h_{21} = h_{22}$	$\dot{E}x_{26}$, $\dot{E}x_5$, $\dot{E}x_{21}$	$\dot{E}x_6$, $\dot{E}x_{27}$, $\dot{E}x_{22}$	---
Mixer 2	$\dot{m}_7 h_7 + \dot{m}_{2\prime\prime} h_{2\prime\prime} = \dot{m}_{7\prime} h_{7\prime}$	$\dot{E}x_7 + \dot{E}x_{2"}$	$Ex_{7\prime}$	---
Splitter1	$\dot{m}_2 h_2 = \dot{m}_{2\prime} h_{2\prime} + \dot{m}_{2"} h_{2"}$	$\dot{E}x_2$	$\dot{E}x_{2\prime} + \dot{E}x_{2"}$	
Splitter2	$\dot{m}_8 h_8 = \dot{m}_{8\prime} h_{8\prime} + \dot{m}_{8"} h_{8"}$	$\dot{E}x_8$	$\dot{E}x_{8\prime} + \dot{E}x_{8"}$	

When low-temperature energy resources are used as sensible heat sources, the fluid temperature decreases due to heat transfer from the hot fluid to the cold one. If a pure fluid is used as the operating fluid, the position of the pinch point occurs simply at the inlet and outlet of the heat exchanger, or the fluid saturation point. On the other hand, when a zeotropic type of fluid, such as an ammonia-water solution, is applied as a working fluid, the solution temperature changes nonlinearly, even under isobaric conditions [15]. Under these circumstances, the evaluation of the pinch point is more complicated than that of the case in which a pure fluid is utilized. To evaluate and analyze the pinch point temperature difference, the specific heat of the working fluid (c_p) is assumed to be constant at the mean temperature [28].

The dimensionless enthalpy (H) is defined as follows [28]:

$$H = \frac{Q}{Q_{\text{total}}} = \frac{h(T, P_{\text{H}}, x_{\text{b}}) - h_{\text{wi}}}{h_{\text{wo}} - h_{\text{wi}}} \tag{49}$$

This parameter is in the range of $0 \leq H \leq 1$. Values $H = 0$ and $H = 1$ represent the boiler inlet and outlet states, respectively. To obtain the location of the pinch point, and the temperature of the boiler exhaust gases, T_{iso}, a specific loop code must be implemented. T_{iso} is predicted by the equation (50) while the temperature difference between the cold and the hot fluid is calculated with the equation (49). The range of H value is divided into 100 equal parts, with the step of 0.01. If the desired pinch temperature difference does not occur at any value of H, a new temperature (T_{iso}) is assumed as the next try. The temperature estimation continues until a pinch point temperature difference is within the range of H. In this case, the estimated temperature is assumed correct and the thermodynamic properties of the fluid leaving the boiler can be obtained.

$$T_{\text{iso}} = T_{\text{wi}} + \Delta T_{\text{pp,B}} + kk\,(i-1) \quad (50)$$

T_{wi} is the temperature of the ammonia-water solution entering the boiler, kk and i are the required parameters to write a loop code in which kk = 0.01, and 1<i<100, and $\Delta T_{\text{pp,B}}$ is the pinch point temperature difference in the boiler.

Additionally, the first and the second law efficiencies of the proposed trigeneration system are calculated as follows:

$$\eta_{\text{I}} = \frac{\dot{W}_{\text{net}} + \dot{Q}_{\text{ref}} + \dot{Q}_{\text{HU}}}{\dot{Q}_{\text{Boiler}} + \dot{Q}_{\text{Reboiler}}} \quad (51)$$

$$\eta_{\text{II}} = \frac{\dot{W}_{\text{net}} + (\dot{E}_{\text{Pr,ref}} + \dot{E}_{\text{Pr,HU}})}{\dot{E}_{40} - \dot{E}_{42}} \quad (52)$$

3. Simulation results and discussion

3.1. Model validation

As mentioned, the proposed system consists of three main subsystems including gasifier, supercritical CO_2 cycle and Kalina cycle. To validate the developed mathematical model for each of these subsystems, the obtained data were compared with available literature data under the same assumptions. First, the validation concerning the gasifier subsystem is demonstrated. Table 6 presents a comparison of the gas composition obtained from the gasification in the present work and those reported in [37] under the same condition. As can be seen, the results are close to each other. Second, to demonstrate the validity of presented formulation for s-CO_2 cycle, the obtained results for temperature, pressure, entropy, enthalpy and mass rate are compared with those presented in [24] at different set points of the s-CO_2 cycle. A good agreement is evident from the data tabulated in Table 6.

Table 6. A comparison of the gas yield obtained from the gasification in the present work and those reported in [37]

Parameter	**Jayah et al.** [37]	**Present work**
H_2 (%)	12.5	18.66
CO_2 (%)	8.5	11.5
CO (%)	18.9	19.14
CH_4 (%)	1.2	0.11
N_2 (%)	59.1	59.1
Lower heating value (MJ/m^3)	4.165	4.47
Air-fuel ratio	2.29	2.6

3.2. Thermodynamic properties and exergy analysis

This subsection investigates the behavior of the proposed system from thermodynamic and exergy perspectives. Table 7 represents the thermodynamic properties of different streams of the proposed system including temperature, pressure, mass fraction of ammonia, mass flow rate, enthalpy, entropy and exergy rate. In this table, MSW and AW refer to municipal solid waste and ammonia-water, in turn. As expected, the working fluid at state 13 and 44 has the highest potential to produce power.

Table 7. Thermodynamic properties of different streams of proposed system

State	Working fluid	T (K)	p (bar)	x (%)	$\dot{m}$ (kg/s)	h (kJ/kg)	s (kJ/kg/K)	$\dot{E}$ (kW)
1	AW	308.2	1.68	0.3408	9.772	-54.91	0.418	65862
2	AW	308.3	4.301	0.3408	9.772	-54.56	0.4184	65864
2′	AW	308.3	4.301	0.3408	7.73	-54.56	0.4184	52102
2″	AW	308.3	4.301	0.3408	2.042	-54.56	0.4184	13762
3	AW	336.4	4.301	0.3408	7.73	68.35	0.7996	52174
3′	AW	348.4	4.301	0.3408	7.73	264.9	1.371	52377
4	AW	349.6	4.301	0.3408	7.73	287	1.434	52403
4′	AW	349.6	4.301	0.2771	6.979	151.1	0.9976	38370
4″	AW	349.6	4.301	0.9329	0.7508	1527	5.421	13990
5	AW	340.9	4.301	0.2771	6.979	112.9	0.8873	38333
6	AW	325.6	1.68	0.2771	6.979	112.9	0.8932	38321
7	AW	319.8	4.301	0.9329	0.7508	1249	4.596	13905
7′	AW	328.3	4.301	0.5	2.793	295.9	1.553	27742
8	AW	308.2	4.301	0.5	2.793	-82.59	0.3672	27672
8′	AW	308.2	4.301	0.5	1.592	-82.59	0.3672	15773
8″	AW	308.2	4.301	0.5	1.201	-82.59	0.3672	11899
9	AW	309.4	86.26	0.5	1.592	-70.82	0.3728	15789
10	AW	346.6	86.26	0.5	1.592	96.65	0.8838	15813
11	AW	458.95	86.26	0.5	1.592	681.2	2.335	16055
12	AW	528.1	86.26	0.5	1.592	2216	5.393	17047
13	AW	653.1	86.26	0.5	1.592	2619	6.079	17364
14	AW	367	1.68	0.5	1.592	1903	6.298	16121
14′	AW	346.9	1.68	0.5	1.592	948.6	3.637	15863
15	AW	311.3	1.68	0.5	1.592	351.8	1.831	15770
16	AW	323.3	1.68	0.3408	9.772	205.5	1.24	66014
17	AW	308.4	13.48	0.5	1.201	-81.27	0.3677	11900
18	AW	346.6	13.48	0.5	1.201	92.55	0.8989	11919
19	AW	326.1	13.48	0.998	0.3854	1341	4.375	7743
20	AW	308.1	13.48	0.998	0.3854	164.6	0.5819	7726
21	AW	267.3	13.48	0.998	0.3854	-27.75	-0.0883	7728
22	AW	250.4	1.68	0.998	0.3854	-27.75	0.07292	7727
23	AW	251.2	1.68	0.998	0.3854	1173	4.699	7641
24	AW	305.1	1.68	0.998	0.3854	1365	5.412	7634
25	AW	398.15	13.48	0.2646	0.8153	373.8	1.582	4317
26	AW	351.4	13.48	0.2646	0.8153	164.8	1.024	4282
27	AW	330.2	1.68	0.2646	0.8153	164.8	1.038	4279
28	Water	298.2	1	-	121.7	104.8	0.3669	304.2
29	Water	303.2	1	-	12.7	125.8	0.4365	326.6
30	Water	298.1	1	-	50.53	104.8	0.3669	126.3

31	Water	303.2	1	-	50.53	125.8	0.4365	135.6
32	Water	298.2	1	-	2.267	104.8	0.3669	5.668
33	Water	303.15	1	-	2.267	125.8	0.4365	6.085
34	Water	298.2	1	-	21.67	104.8	0.3669	54.19
35	Water	303.2	1	-	21.67	125.8	0.4365	58.17
36	Air	260	1	-	94.86	260.1	6.726	4411
37	Air	255.2	1	-	94.86	255.2	6.707	4483
38	Inlet air	298	1	-	3.853	0	0	17.72
39	Produced gas	823	1	-	3.683	-2882	1.775	10878
40	Exhaust gas	1555	1	-	7.536	-1437	2.218	7881
41	Exhaust gas	821.2	1	-	7.536	-2389	1.395	2555
42	Exhaust gas	353.4	1	-	7.536	-2922	0.4434	677.2
43	s-CO_2	606.6	345.8	-	26.36	241.4	-0.5096	22293
44	s-CO_2	818.2	338.9	-	26.36	513.7	-0.1204	26410
45	s-CO_2	653.6	75	-	26.36	338.7	-0.06821	21390
46	s-CO_2	529.5	72.75	-	26.36	198.7	-0.3001	19520
47	s-CO_2	373.5	71.3	-	26.36	20.07	-0.6974	17933
48	s-CO_2	373.5	71.3	-	7.907	20.07	-0.6974	5380
49	s-CO_2	373.5	71.3	-	18.45	20.07	-0.6974	12553
50	s-CO_2	300.7	68.47	-	18.45	-221.5	-1.457	12275
51	s-CO_2	343.8	342.4	-	18.45	-179.1	-1.438	12948
52	s-CO_2	488.9	356.5	-	18.45	75.98	-0.8192	14254
53	s-CO_2	547.5	356.5	-	7.907	160.5	-0.6557	6392
54	s-CO_2	505.9	356.5	-	26.36	101.3	-0.7682	20631
55	s-CO_2	342.2	69.87	-	18.45	-21	-0.8093	12411
56	Water	298.2	1	-	62.76	104.8	0.3669	156.9
57	Water	312.2	1	-	62.76	163.8	0.5601	243.5
58	Air	298	1	-	2.71	0	0	12.47
59	MSW	298	1	-	1.155			18908

According to Table 8, based on the conducted analysis it can be concluded that the combustion chamber and gasifier subsystem, the s-CO_2 cycle, and the Kalina cycle contribute to 76%, 17%, and 7%, respectively, of all exergy destruction in the proposed system. Therefore, the combustion chamber and gasifier subsystem have by far the most contribution to the exergy destruction. As can be seen from Table 8, after gasifier and combustion chamber components, generator has the highest amount of exergy destruction. Furthermore, mixer, distillation column, separator, sub-cooler, valves 2, 4 and 5 and heating unit are the most efficient components from exergy viewpoint. Additionally, absorber 1, absorber 2, preheater 2 and condenser 1 are the most exergy deficient components among all the components of the system.

Table 8. Exergy destruction and efficiency of different components of proposed trigeneration system

Component	**Exergy destruction (kW)**	**Exergy efficiency (%)**
Boiler	326.1	60.72

Kalina Turbine	104.1	91.63
Recuperator 1	75.81	78.38
Recuperator 2	9.181	73.64
Mixer	0.023	100
Absorber 1	129.6	14.72
Absorber 2	60.89	13.24
Pump 1	1.161	66.27
Pump 2	2.689	85.64
Pump 3	0.1966	87.58
Preheater 1	12.87	65.27
Preheater 2	66.25	21.97
Distillation column	0.2115	100
Condenser 1	13.66	22.59
Seperator	128	99.76
Subcooler	4.944	99.97
Evaporator	12.6	85.22
Throttling Valle 2	12.31	99.97
Throttling Valle 4	3.397	99.92
Throttling valve 5	1.766	99.98
Generator	1209	77.3
Turbine 1	409.6	91.84
HTR	209.1	88.83
LTR	280.2	82.34
MC	109	86.06
RC	98.16	91.16
Heating unit	49.2	99.61
Combustion chamber	2839	72.33
Gasifier	7604	57.49

3.3. Parametric study

In each analysis of energy generation systems there are some main objectives that should be maximized or minimized. Thus, in this section, a parametric study is conducted in order to assess the impact of several important parameters on the net electricity production and exergy efficiency. In this way, it is possible to find variables that have the highest potential for improving the system's performance. In this study split fraction ration, Kalina turbine isentropic efficiency, pinch point temperature difference of boiler, Kalina turbine inlet pressure, mixture quality of the output at the bottom of the distillation column, air-fuel ratio, supercritical CO_2 turbine efficiency, pressure ratio of the compressors and pinch point temperature difference of the generator were selected as decision variables. Figures 2 to 10 presents the most important results of the conducted analysis.

As it results from Figure 2, by increasing $f_{w,}$ which is the mass flow rate of stream 9 to that of stream 8, the mass flow for the power generation exceeds the mass flow entering the refrigeration system. So, the work performed by the turbine increases causing an enhancement in exergy

efficiency. While if this increase is applied to the other side of refrigeration, it does not have much effect on the exergy efficiency, which would cause a decrease in the rate of net output electricity.

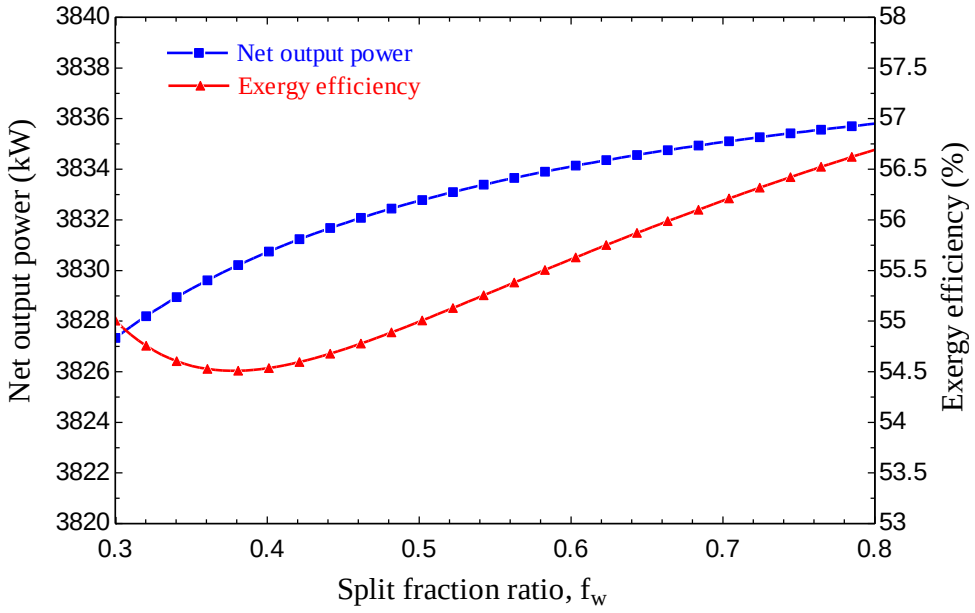

Figure 2. Spilt fraction ratio, f_w to exergy efficiency and net output power

Figure 3 shows the effect of the pinch point temperature difference of boiler on two factors. With an increase of this temperature difference, irreversibility in the boiler increases. As the temperature difference in the heat exchanger increase, the process moves away from the quasi-equilibrium process, which causes entropy creation and irreversibility in the boiler. In turn, irreversibility causes the destruction of exergy in the system and reducing power production.

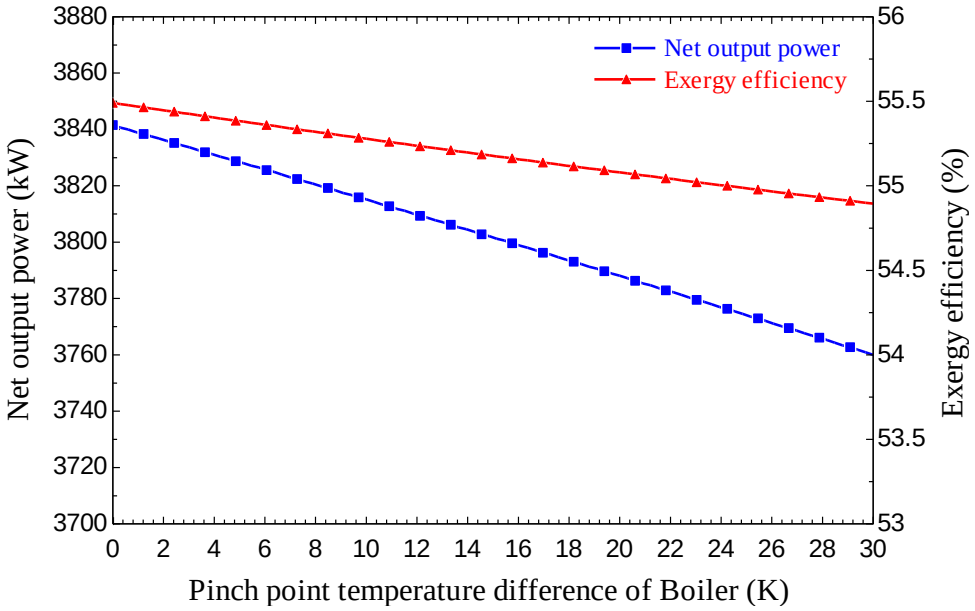

Figure 3. Influence of the boiler pinch point temperature difference on the exergy efficiency and the net output power of the system

Figure 4 shows the effect of Kalina inlet pressure on the exergy efficiency and power production. An increase of the inlet pressure causes high-temperature flow and high enthalpy, which in turn causes an increase in turbine power production and in the second law efficiency. An increase in the turbine inlet pressure, obviously, causes an increase in the pump's power consumption. However, the pump's power consumption is slightly lower than the turbine power production. Actually, because of this, power production and exergy efficiency increase.

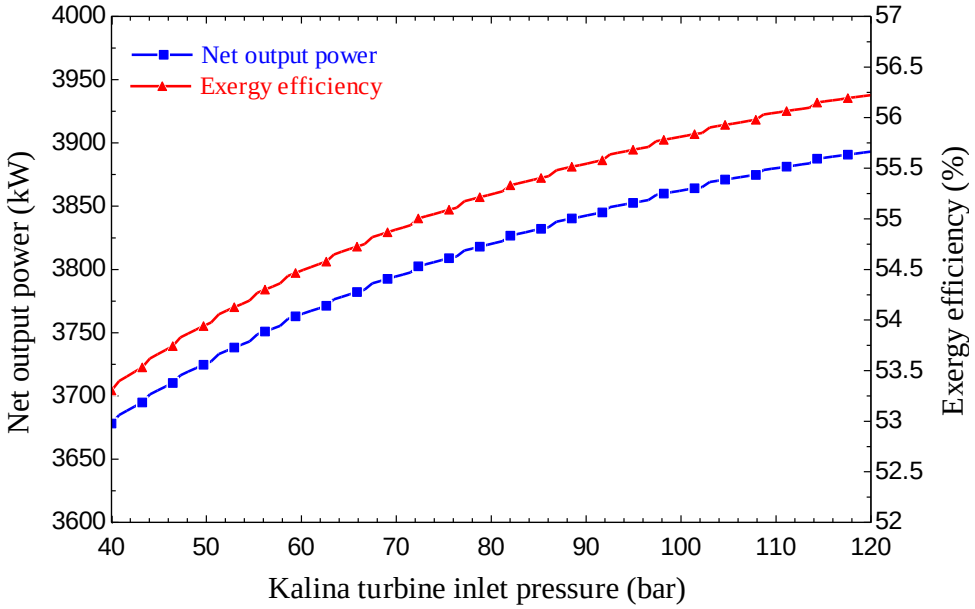

Figure 4. Influence of the Kalina turbine inlet pressure on the exergy efficiency and the net output power

Figure 5 presents the effect of the vapor fraction (Qu_{25}) at the bottom of the distillation column. With an increase in the vapor fraction, thermal losses in the distillation column increase, and the efficiency of refrigerant separation from the mixture (ammonia from water) decreases, which means an increase in irreversibility. Because of this, which is evident from the figure, exergy efficiency decreases with an increase in Qu_{25}. As the streams entering the absorption cooling section and Kalina turbine do not affect each other, an increase in the vapor fraction does not have much impact on the power production, so it is constant.

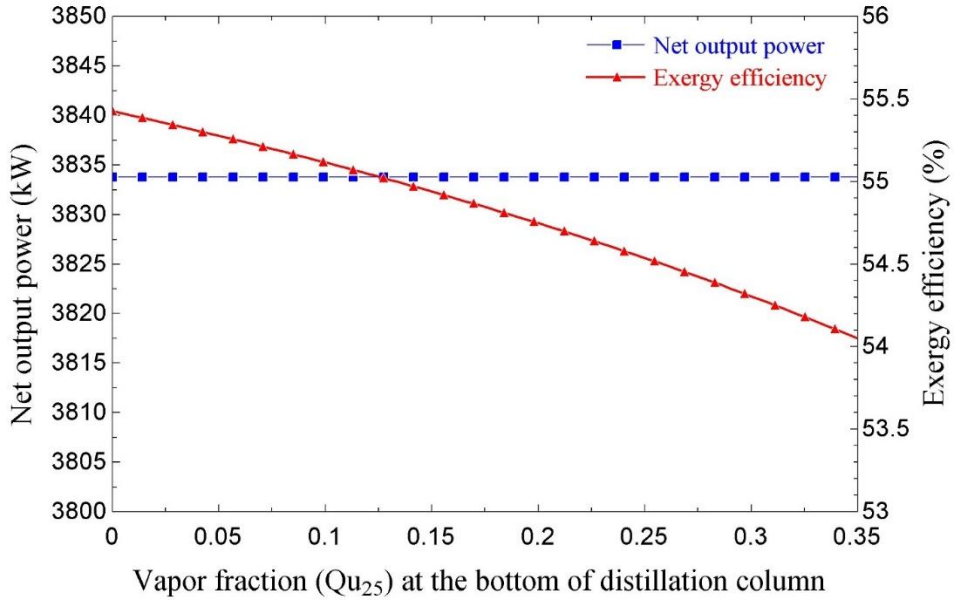

Figure 5. Influence of the vapor fraction (Qu_{25}) on the exergy efficiency and the net output power

Figure 6 presents an influence of the molar equivalence ratio on the two analyzed quantities. With the increase of molar equivalence ratio, the net power output increases and the exergy efficiency decreases. With the increase in φ, there will be less air in combustion feed, causing the creation of high-temperature exhaust gases and high energy at the inlet of the Kalina turbine and s-CO_2 turbine. Consequently, the net output power is increasing. However, high-temperature combustion products result in an enhancement of the irreversibility in such components as combustion chamber, generator and boiler. This, in turn, causes a decrease in the exergy efficiency.

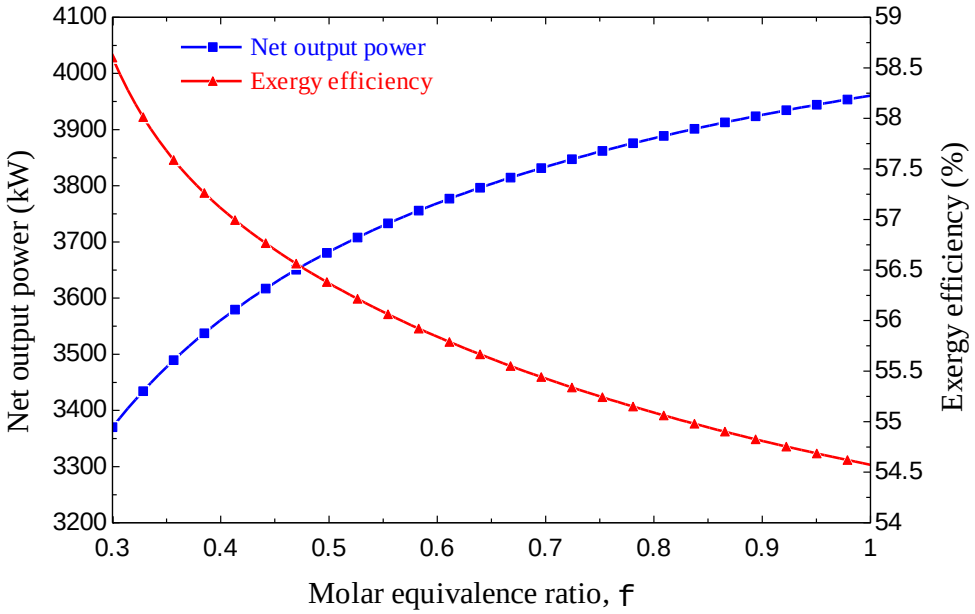

Figure 6. Influence of the molar equivalence ratio on the exergy efficiency and net output power

In Figure 7 the effect of the s-CO_2 turbine isentropic efficiency on the net output power and the exergy efficiency is presented. With the increase in isentropic efficiency, irreversibility in the turbine decreases, which causes an increase in turbine power production. Followed by this, exergy efficiency improves and increases.

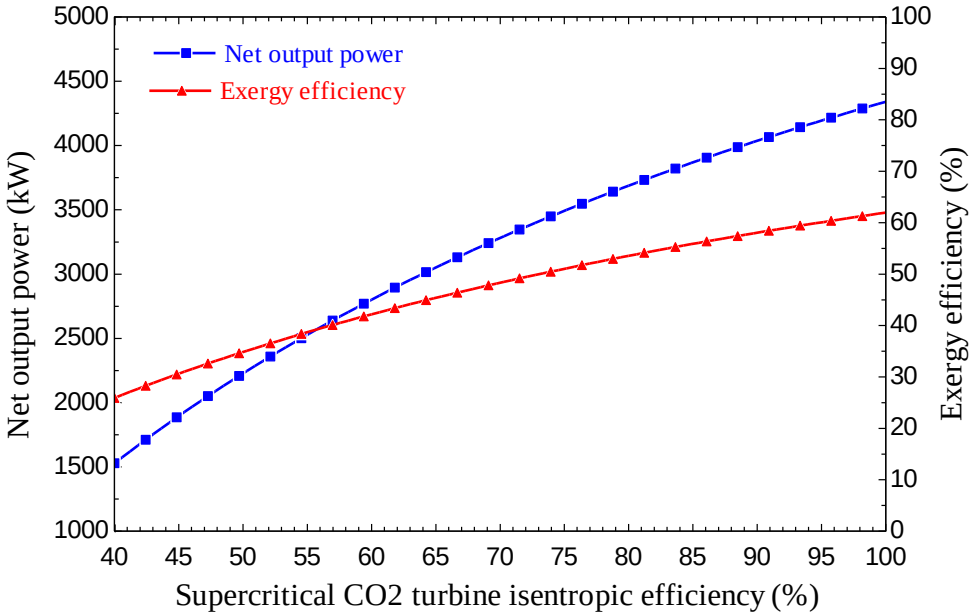

Figure 7. Influence of the supercritical CO_2 turbine isentropic efficiency on the exergy efficiency and net output power

Figure 8 shows the effect of the pressure ratio of the compressors in the s-CO_2 cycle. An increase in the pressure ratio of the compressors causes an increase in the turbine inlet flow pressure. This in turn causes an increase of the work generated in the turbine and an increase in the exergy efficiency. Further increase of the pressure ratio over 5 causes a decrease in the net power production and the exergy efficiency. This is because the increase of the pressure ratio to higher values causes an increase in the compressor's power consumption and, in fact, increases input exergy and, therefore, a reduction in exergy efficiency and net power production.

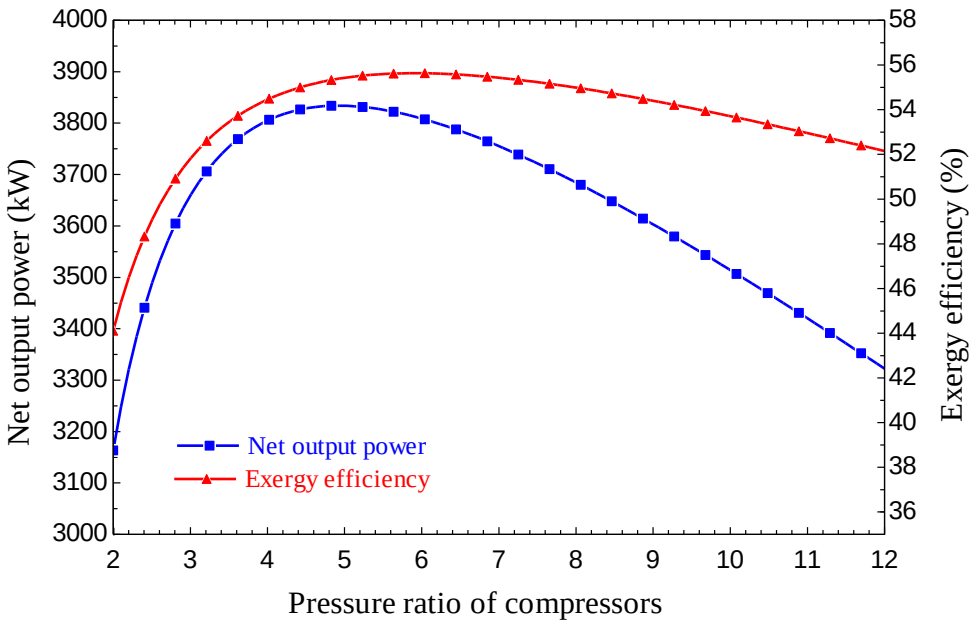

Figure 8. Influence of the pressure ratio of the compressors on the exergy efficiency and net output power

3.4. Comparison of the results with previous works

In Table 9, the results obtained from the current work are compared with the results from the four related research done before. Four parameters in this chart, i.e., energy efficiency, exergy efficiency, net produced electricity, and refrigeration capacity, were examined. In order to compare the configurations, Ref. [38] uses a single effect absorption chiller for district cooling and an engine as a heat source while the current work exploits a double effect absorption chiller and a biomass gasifier. In addition, Ref. [15] proposed a modified Kalina cycle using waste heat from an engine, but the present work added a s-CO_2 power cycle driven by a biomass gasifier. What is more, Ref. [20] takes advantage of a gas turbine and a single effect absorption chiller for a trigeneration cycle, whereas, the current study benefits from a s-CO_2 power cycle and a modified Kalina cycle. Additionally, Ref. [39] designed a geothermal-based simple Kalina system. In contrast, the present research is driven by a biomass gasification unit for a modified Kalina cycle. As results from this comparison, the proposed system has better performance than other solutions presented in the literature in terms of thermodynamics, which confirms that it is a perspective solution for generation of heat, cold and electricity.

Table 9. Comparison of the results from present work with other studies

Present work vs. previous works	Energy efficiency (%)	Exergy efficiency (%)	Net electricity rate (kW)	Cooling capacity (kW)
Present work	71.45	55.43	3834	462.8

Wu et al. [38]	40.38	54.02	257.43	113.26
Kalan et al. [15]	27.96	53.19	412.6	177
Asgari et al. [20]	66.98	27.92	30000.0	39240
Kordlar et al. [39]	10.34	23.13	910.8	996.3

4. Conclusion

From the conducted analysis the following conclusions can be drawn:

- The proposed trigeneration system is composed of three main parts. The input energy is provided by municipal solid waste (although other types of waste fuels can possible be used), which eliminates the need for fossil fuels. A large portion of the power is generated by the s-CO_2 cycle (called the high-temperature cycle). Due to its optimized concentration capability, the modified Kalina cycle is responsible for refrigeration.
- Energy and exergy analyses revealed that for the mass flow rate of 3.383 kg/s of fuel and the exhaust gas temperature of 1,555 K, the first and second law thermodynamic efficiency were 71.45 and 55.43%, respectively. The total generated power was 3,834 kW, of which 2,694 kW was produced by the s-CO_2 cycle, and the remaining power (i.e., 1,140 kW) was generated by the Kalina cycle. The cold generated by the evaporator was 4,628 kW and the heat received by the heating unit (HU) was 3,699 kW.
- Regarding the integrated exergy analysis for the whole system, the maximum losses are connected to the gasifier-combustion chamber system, 76% of the total losses, among the s-CO_2 cycle, Kalina cycle, and gasifier-combustion chamber system. On the other hand, the maximum loss of exergy was equal to 7,604 kW, 2,839 kW, and 1,209 kW for the gasifier, combustion chamber, and generator, respectively. The total loss of exergy was calculated as 23,626 kW. Each component of the system was analyzed in terms of exergy. The maximum exergy efficiency was achieved by mixer and distillation column, respectively, while the minimum exergy efficiency was calculated for the absorber 2 (13.24%) and absorber 1 (14.72%).
- Among the possible parameters governing the system, the effect of nine critical parameters on two important factors, i.e., the net power output rate and exergy destruction was assessed. As the isentropic efficiency of Kalina turbine, Kalina inlet pressure, and the isentropic efficiency of s-CO_2 turbine increased, net power output and exergy destruction both increased. The most prominent parameter affecting the net electricity rate and exergy destruction was the isentropic efficiency of the s-CO_2 turbine. As the pinch point temperature difference of the boiler and the generator increased, both parameters were reduced due to the increased losses.
- The results also indicated that for higher air-fuel ratios, the exergy efficiency was reduced while the net electricity rate increased. It is worth noting that for the specified range of the compression ratios, the optimal ratio was around 5. Hence, both net electricity rate and

exergy destruction began to fall for ratios smaller than 5. When the quality of the operating fluid exiting the bottom of the distillation column was higher, the exergy efficiency parameter experienced a similar declining trend.

To sum up, the proposed new configuration of a biomass-based integrated cooling, heating, and power system is analyzed from energy and exergy perspectives for efficiency improvement. This system can be designed and exploited in a myriad of communities for district heating, district cooling and electricity network. In the future works, we will examine further the system to improve its efficiency by assessing various types of gasifiers and s-CO_2 power cycle. It is also planned to assess and optimize the proposed system from an economic and environmental point of view.

References

[1] Ahmadi R, Jokar H, Motamedi M. A solar pressurizable liquid piston stirling engine: Part 2, optimization and development. Energy 2018;164:1200–15.

[2] Uchman W, Skorek-Osikowska A, Jurczyk M, Węcel D. The analysis of dynamic operation of power-to-SNG system with hydrogen generator powered with renewable energy, hydrogen storage and methanation unit. Energy 2020;213:118802.

[3] Katla D, Jurczyk M, Skorek-Osikowska A, Uchman W. Analysis of the integrated system of electrolysis and methanation units for the production of synthetic natural gas (SNG). Energy 2021;237:121479.

[4] Ghiasirad H, Asgari N, Khoshbakhti Saray R, Mirmasoumi S. Thermoeconomic assessment of a geothermal based combined cooling, heating, and power system, integrated with a humidification-dehumidification desalination unit and an absorption heat transformer. Energy Convers Manag 2021;235:113969.

[5] Skorek-Osikowska A, Kotowicz J, Uchman W. Thermodynamic assessment of the operation of a self-sufficient, biomass based district heating system integrated with a Stirling engine and biomass gasification. Energy 2017;141:1764–78.

[6] Ghiasirad H, Rostamzadeh H, Nasri S. Design and Evaluation of a New Solar Tower-Based Multi-generation System: Part I, Thermal Modeling. Integr. Clean Sustain. Energy Resour. Storage Multi-Generation Syst., Cham: Springer International Publishing; 2020, p. 83–102.

[7] Cheng Z, Wang J, Yang P, Wang Y, Chen G, Zhao P, et al. Comparison of control strategies and dynamic behaviour analysis of a Kalina cycle driven by a low-grade heat source. Energy 2022;242:122958.

[8] Javanfam F, Ghiasirad H, Khoshbakhti Saray R. Efficiency Improvement and Cost Analysis of a New Combined Absorption Cooling and Power System. In: Amidpour M, Ebadollahi M, Jabari F, Kolahi M-R, Ghaebi H, editors. Synerg. Dev. Renewables Assist. Multi-carrier Syst., Cham: Springer International Publishing; 2022, p. 23–50.

[9] Skorek-Osikowska A, Bartela Ł, Kotowicz J, Sobolewski A, Iluk T, Remiorz L. The influence of the size of the CHP (combined heat and power) system integrated with a biomass fueled gas generator and piston engine on the thermodynamic and economic effectiveness of electricity and heat generation. Energy 2014;67:328–40.

[10] Huang Y, Wang YD, Rezvani S, McIlveen-Wright DR, Anderson M, Mondol J, et al. A techno-economic assessment of biomass fuelled trigeneration system integrated with organic Rankine cycle. Appl Therm Eng 2013;53:325–31.

[11] He F, Liu X, Wang M, Zhou S, Heydarian D. Energy, exergy, exergoeconomic, and environmental analyses and multi-objective optimization of a biomass-to-energy integrated thermal power plant. Alexandria Eng J 2022;61:5629–48.

[12] Cao Y, Habibi H, Zoghi M, Raise A. Waste heat recovery of a combined regenerative gas turbine - recompression supercritical CO2 Brayton cycle driven by a hybrid solar-biomass heat source for multi-generation purpose: 4E analysis and parametric study. Energy 2021;236:121432.

[13] Musharavati F, Khanmohammadi S, Pakseresht A. Proposed a new geothermal based poly-generation energy system including Kalina cycle, reverse osmosis desalination, elecrolyzer amplified with thermoelectric: 3E analysis and optimization. Appl Therm Eng 2021;187:116596.

[14] Ji-chao Y, Sobhani B. Integration of biomass gasification with a supercritical CO2 and Kalina cycles in a combined heating and power system: A thermodynamic and exergoeconomic analysis. Energy 2021;222:119980.

[15] Kalan AS, Ghiasirad H, Saray RK, Mirmasoumi S. Thermo-economic evaluation and multi-objective optimization of a waste heat driven combined cooling and power system based on a modified Kalina cycle. Energy Convers Manag 2021;247:114723.

[16] Fan G, Dai Y. Thermo-economic optimization and part-load analysis of the combined supercritical CO2 and Kalina cycle. Energy Convers Manag 2021;245:114572.

[17] Gholamian E, Mahmoudi SMS, Zare V. Proposal, exergy analysis and optimization of a new biomass-based cogeneration system. Appl Therm Eng 2016;93:223–35.

[18] Wang J-J, Yang K, Xu Z-L, Fu C. Energy and exergy analyses of an integrated CCHP system with biomass air gasification. Appl Energy 2015;142:317–27.

[19] Ghiasirad H, Rostamzadeh H, Nasri S. Design and Evaluation of a New Solar Tower-Based Multi-generation System: Part II, Exergy and Exergoeconomic Modeling. Integr. Clean Sustain. Energy Resour. Storage Multi-Generation Syst., Cham: Springer International Publishing; 2020, p. 103–20.

[20] Asgari N, Khoshbakhti Saray R, Mirmasoumi S. Energy and exergy analyses of a novel seasonal CCHP system driven by a gas turbine integrated with a biomass gasification unit and a LiBr-water absorption chiller. Energy Convers Manag 2020;220:113096.

[21] Ghiasirad H, Saray RK, Abdi B, Bahlouli K. Detailed 3E Exploration of a Sugar Industry Using Its Experimental Data. In: Amidpour M, Ebadollahi M, Jabari F, Kolahi M-R, Ghaebi H, editors. Synerg. Dev. Renewables Assist. Multi-carrier Syst., Cham: Springer International Publishing; 2022, p. 391–429.

[22] Li H, Jin Z, Yang Y, Huo Y, Yan X, Zhao P, et al. Preliminary conceptual design and performance assessment of combined heat and power systems based on the supercritical carbon dioxide power plant. Energy Convers Manag 2019;199:111939.

[23] Mohammed RH, Qasem NAA, Zubair SM. Enhancing the thermal and economic

performance of supercritical CO2 plant by waste heat recovery using an ejector refrigeration cycle. Energy Convers Manag 2020;224:113340.

[24] Mohammadi Z, Fallah M, Mahmoudi SMS. Advanced exergy analysis of recompression supercritical CO2 cycle. Energy 2019;178:631–43.

[25] Alharbi S, Elsayed ML, Chow LC. Exergoeconomic analysis and optimization of an integrated system of supercritical CO2 Brayton cycle and multi-effect desalination. Energy 2020;197:117225.

[26] Cao Y, Dhahad HA, Togun H, Anqi AE, Farouk N, Farhang B. Proposal and thermo-economic optimization of using LNG cold exergy for compressor inlet cooling in an integrated biomass fueled triple combined power cycle. Int J Hydrogen Energy 2021;46:15351–66.

[27] Heidari M, Ataei A, Rahdar MH. Development and analysis of two novel methods for power generation from flare gas. Appl Therm Eng 2016;104:687–96.

[28] Zhang S, Chen Y, Wu J, Zhu Z. Thermodynamic analysis on a modified Kalina cycle with parallel cogeneration of power and refrigeration. Energy Convers Manag 2018;163:1–12.

[29] Khaljani M, Saray RK, Bahlouli K. Comprehensive analysis of energy, exergy and exergo-economic of cogeneration of heat and power in a combined gas turbine and organic Rankine cycle. Energy Convers Manag 2015;97:154–65.

[30] Rostamzadeh H, Ghiasirad H, Amidpour M, Amidpour Y. Performance enhancement of a conventional multi-effect desalination (MED) system by heat pump cycles. Desalination 2020.

[31] Bejan A, Tsatsaronis G, Maran M. Thermal design and optimization. Wiley, John; 1996.

[32] Behzadi A, Gholamian E, Houshfar E, Habibollahzade A. Multi-objective optimization and exergoeconomic analysis of waste heat recovery from Tehran's waste-to-energy plant integrated with an ORC unit. Energy 2018;160:1055–68.

[33] Behzadi A, Arabkoohsar A, Gholamian E. Multi-criteria optimization of a biomass-fired proton exchange membrane fuel cell integrated with organic rankine cycle/thermoelectric generator using different gasification agents. Energy 2020;201:117640.

[34] Zainal ZA, Ali R, Lean CH, Seetharamu KN. Prediction of performance of a downdraft gasifier using equilibrium modeling for different biomass materials. Energy Convers Manag 2001.

[35] Jarungthammachote S, Dutta A. Thermodynamic equilibrium model and second law analysis of a downdraft waste gasifier. Energy 2007;32:1660–9.

[36] Katla D, Bartela Ł, Skorek-Osikowska A. Evaluation of electricity generation subsystem of power-to-gas-to-power unit using gas expander and heat recovery steam generator. Energy 2020;212:118600.

[37] Jayah TH, Aye L, Fuller RJ, Stewart DF. Computer simulation of a downdraft wood gasifier for tea drying. Biomass and Bioenergy 2003;25:459–69.

[38] Wu C, Xu X, Li Q, Li J, Wang S, Liu C. Proposal and assessment of a combined cooling and power system based on the regenerative supercritical carbon dioxide Brayton cycle

integrated with an absorption refrigeration cycle for engine waste heat recovery. Energy Convers Manag 2020;207:112527.

[39] Akbari Kordlar M, Mahmoudi SMS. Exergeoconomic analysis and optimization of a novel cogeneration system producing power and refrigeration. Energy Convers Manag 2017;134:208–20.

26.07.2022

Anna Skorek-Osikowska
Silesian University of Technology
Department of Power Engineering and Turbomachinery
ul. Konarskiego 18, Gliwice, Poland
+48 32 2372524
anna.skorek@polsl.pl

Dear Editor,

I would like to submit the paper entitled "**Biomass-to-energy integrated trigeneration system using supercritical CO_2 and modified Kalina cycles: energy and exergy analysis**", jointly written by Ali Shokri Kalan, Shadab Heidarabadi, Mohammad Khaleghi, Hamed Ghiasirad, Anna Skorek-Osikowska, to be published as a full-length article in Energy journal.

Gasification of biomass is one of the most widely used thermochemical conversion methods for producing renewable energy, fuels, and biochar. This study presents a novel trigeneration system for heat, cold and electricity production. The proposed system involves biomass gasification, a supercritical CO_2 cycle and a Kalina cycle. Utilizing a modified Kalina cycle together with s-CO_2 cycle is a key advantage of the proposed system. To increase the system's flexibility under different operating conditions, the Kalina cycle uses an ammonia-water mixture as the working fluid. Since the ammonia-water mixture vaporizes non-isothermally, the Kalina cycle is better than the conventional Rankine cycle. Despite this, the feasibility of the proposed biomass-powered system has not been investigated so far. A novel combined cooling, heating and power generation (CCHP) system including a biomass gasifier, Kalina cycle, s-CO_2 cycle, and utilization of supercritical carbon dioxide for power generation, as well as energy, exergy evaluation of the proposed system are the most notable contributions of this work.

The main novelties of the proposed system can be summarized as follows:

- Using a reboiler heater and a heating unit in s-CO_2 power cycle rather than a condenser,
- Serial configuration of syngas stream to recover more thermal energy,
- Carbon dioxide utilization in the first cycle,
- Energy and exergy analysis to improve the most destructive subsystems,
- Combining two efficient cycles to meet cooling, heating, and power demands,
- Using municipal solid waste gasification as an alternative energy sources,
- Conducting parametric study using net output power and exergy efficiency as objective functions in order to find the decision variables.

I assert that this study is original and has not been published or submitted to other journals. There are no conflicts of interest related to this work, and there has been no crucial financial aid for this study that could have affected its results. As corresponding author, I am sure that the text has been read and approved for submission by all the authors.

We hope our research is appropriate to be published and look forward to hearing from you.

Your sincerely,

Anna Skorek-Osikowska

The authors declare that they have no known competing financial interests or personal relationships that could have appeared to influence the work reported in this paper.

Highlights:

- A biomass driven combined cooling, heating, and power system is proposed.
- Gasifier, combustion chamber, and generator have the highest irreversibilities.
- Absorbers and preheater 2 have the lowest exergy efficiencies.
- Pressure ratio of compressors should be 5 to maximize the net output power and efficiency.
- Compared to 4 other studies, energy and exergy efficiencies have been improved by 6.67% and 2.61%, respectively.